

CHORUS

This is the accepted manuscript made available via CHORUS. The article has been published as:

Superstrengthening Bi₂Te₃ through Nanotwinning

Guodong Li, Umut Aydemir, Sergey I. Morozov, Max Wood, Qi An, Pengcheng Zhai, Qingjie Zhang, William A. Goddard, III, and G. Jeffrey Snyder

Phys. Rev. Lett. **119**, 085501 — Published 25 August 2017

DOI: [10.1103/PhysRevLett.119.085501](https://doi.org/10.1103/PhysRevLett.119.085501)

Superstrengthening Bismuth Telluride (Bi_2Te_3) through Nanotwinning

Guodong Li ^{1,2}, Umut Aydemir ¹, Sergey I. Morozov ³, Max Wood ¹, Qi An ^{*,4}, Pengcheng Zhai², Qingjie Zhang ^{*,2}, William A. Goddard III ⁵, and G. Jeffrey Snyder ^{*,1}

¹Department of Materials Science and Engineering, Northwestern University, Evanston, Illinois 60208, USA.

²State Key Laboratory of Advanced Technology for Materials Synthesis and Processing, Wuhan University of Technology, Wuhan 430070, China.

³Department of Computer Simulation and Nanotechnology, South Ural State University, Chelyabinsk 454080, Russia

⁴Department of Chemical and Materials Engineering, University of Nevada, Reno, Reno, Nevada, 89557, USA.

⁵Materials and Process Simulation Center, California Institute of Technology, Pasadena, California 91125, USA.

*Corresponding authors: jeff.snyder@northwestern.edu; zhangqj@whut.edu.cn; qia@unr.edu

Abstract: Bismuth telluride (Bi_2Te_3) based thermoelectric (TE) materials have been commercialized successfully as solid-state power generators, but their low mechanical strength suggests that these materials may not be reliable for long-term use in TE devices. Here we use density functional theory (DFT) to show that the ideal shear strength of Bi_2Te_3 can be significantly enhanced up to 215 % by imposing nanoscale twins. We reveal that the origin of the low strength in single crystalline Bi_2Te_3 is the weak **van der Waals** interaction between the Te1 coupling two Te1–Bi–Te2–Bi–Te1 five-layer quint substructures. However we demonstrate here a surprising result that forming twin boundaries between the Te1 atoms of adjacent quint greatly strengthens the interaction between them, leading to a tripling of the ideal shear strength in nanotwinned Bi_2Te_3 (0.6 GPa) compared to that in the single crystalline material (0.19 GPa). This grain boundary engineering strategy opens a new pathway for designing robust Bi_2Te_3 TE semiconductors for high-performance TE devices.

The continued use of fossil fuels to satisfy escalating global energy requirements is causing severe unacceptable environmental impact. This has generated renewed interest in thermoelectric (TE) conversion technology to convert waste heat directly into electricity, which involves no CO₂ production, is scalable to large power plants, and involves no moving parts (silent) [1]. Over the past two decades, the conversion efficiency (zT) of TE materials has enhanced remarkably approaching to ~ 1.8 [2-4], putting TE materials on the threshold of commercial applications. However, under severe operation conditions, TE materials suffer from unavoidable thermo-mechanical stresses from cycling of the temperature gradients, leading to rapid deterioration of material performance and accelerated failure of TE devices [5-7]. In order for thermoelectrics to play a significant role in engineering applications to alternative energy, the strength and the toughness must be dramatically enhanced.

Industrial low temperature waste heat accounts for almost one third of total energy consumption [8]. The bismuth telluride (Bi₂Te₃) state-of-the-art TE material has been widely used for TE refrigeration in this temperature range (300 – 550 K) [9], and is now being considered in the automotive industry for recovering waste heat from exhaust systems. Traditional elemental doping strategies have been successful in significantly improving TE properties [10,11], but they have had little effect on enhancing the mechanical properties [12]. Recently, nano-SiC particles dispersed in Bi₂Te₃ was reported to enhance mechanical strength compared to pure Bi₂Te₃, but with concomitant deterioration of the electronic transport properties [13].

A well-known mechanism for strengthen metal alloys is to increase the number of such interfacial boundaries as grain boundaries (GBs) and twin boundaries (TBs). These boundaries can strengthen the material by pinning dislocations to impede their movement. One way of achieving increased strength is to increase the density of GBs by reducing grain size, the Hall-Petch effect [14,15]. However, below a critical size, sliding or migration of GBs dominates the deformation mechanism, leading to reduced material strength [16,17]. This grain size effect has been widely examined in metal alloys and ceramics [18-20]. but not in nanocrystalline semiconductors. TBs are expected to have a much lower formation energy than GBs, making TBs more stable than GBs, which can make them more effective in strengthening materials [21]. For example, ultrafine-grained Cu with nanoscale twins embedded in individual grains leads to a superstrength relative to conventional coarse-grained polycrystalline Cu [22]. In addition, nanotwins in ceramics have been found to dramatically enhance the hardness of diamond and boron nitride [23,24]. However, influence of nanotwins on the mechanical properties of TE semiconductors remains largely unexplored.

Very recently, a GBs engineering strategy has been proposed to reduce the lattice thermal conductivity and thereby significantly enhance the zT value of TE semiconductors [25-28]. In particular, the dense dislocation arrays formed at low-energy GBs from liquid-phase compaction in bismuth telluride based TE materials has been demonstrated to dramatically decrease the thermal conductivity resulting in a dramatically improved zT of 1.86 at 320 K [25]. This GB strategy has been further applied in other TE semiconductors such as PbTe, Mg₂Si, and CoSb₃ for enhancing their zT values [26-28]. In addition, nanotwinned bismuth telluride also can promote superior TE performance and robust mechanical properties [29], which further suggests that nanoscale twins may play an essential role in the mechanical properties of TE semiconductors.

Here we use the Perdew-Burke-Ernzerhof (PBE) density functional with the D3 **van der Waals** correction to examine the shear stress-strain relationship of single crystalline and nanotwinned bismuth telluride (Bi₂Te₃). We find that the weak **van der Waals** interactions between the Te1 atoms dominate the failure process of crystalline Bi₂Te₃, leading to a very low ideal shear strength of 0.19 GPa. However, we show that the presence of nanoscale twins leads to increased covalency in the Te1 bonds between adjacent quints at the twin boundary, which significantly improves the structural stiffness. This strengthening mechanism results in a dramatically improves the ideal shear strength to 0.60 GPa for nanotwinned Bi₂Te₃, triple the value (0.19 GPa) for single crystalline Bi₂Te₃.

All density functional theory (DFT) simulations were performed using the periodic code Vienna *ab initio* Simulation Package (VASP) with plane wave basis sets [30-32], adopting the projector augmented wave (PAW) method and the Perdew-Burke-Ernzerhof (PBE) exchange-correlation functional applied to account for the core-valence interactions [33]. We showed that an energy cutoff of 600 eV with a (10×10×2) Monkhorst-Pack grid in the k -point reciprocal space sampling give excellent convergence on energy and geometries. The convergence for the electronic self-consistent field and the force criterion were set to less than 1×10^{-6} eV and 1×10^{-2} eV/Å, respectively. Spin-orbit coupling (SOC) was included in the structural optimization of Bi₂Te₃.

To examine the failure mechanism, we applied pure shear deformation by imposing the shear strain on a particular shear direction while allowing full structural relaxation along the other five strain components. The residual stresses for relaxation along the other strain components are all set to less than 0.1 GPa [34].

Bi₂Te₃ crystallizes in a rhombohedral structure with the space group $R\bar{3}m(D_{3d}^5)$, which can be visualized as a hexagonal lattice cell made of Te1–Bi–Te2–Bi–Te1 five-layer (quint)

substructures along the [001] axis as shown in Figure 1(a) [35,36]. The shorter covalent Bi–Te1 (3.11 Å) and longer (weaker) covalent Bi–Te2 (3.30 Å) bonds stabilize the quint five-layer substructure, while the quint is coupled via **van der Waals** interaction between Te1 atom of adjacent quint ($d_{\text{Te1-Te1}} = 3.82$ Å). These weak **van der Waals** interactions control the ease of cleavage along the (00 l) axis [35,36]. PBE gives equilibrium lattice parameters of $a = 4.47$ Å and $c = 31.15$ Å. These values agree well with the previous results ($a = 4.45$ Å, $c = 31.15$ Å) using PBE functional [37], and are only 1.8% and 3.3% larger than the experimental values of $a = 4.39$ Å and $c = 30.50$ Å at 300 K, respectively [38].

Here, we used DFT to determine the atomic structures of three nanotwinned Bi₂Te₃, with TBs lying along

- The {702} plane, see Figure 1(b), leading to an interfacial energy of 325.6 mJ/m². The TB along the {702} plane contains 60×Bi and 90×Te atoms. The measured angle on each side of the TBs is 37°, and the twinning size is 2.4 nm. Along the TB plane of {702}, two new covalent Te1–Te1 bonds (3.48 Å) are formed, further coupling adjacent Te1–Bi–Te2–Bi–Te1.
- The {70 $\bar{1}$ } plane, see Figure S1 [39], leading to an interfacial energy of 385.7 mJ/m².
- The {210} plane, see Figure S2 [39], leading to an interfacial energy of 440.7 mJ/m².

These three nanotwinned Bi₂Te₃ have been experimentally observed recently [29,40].

To understand the intrinsic failure mechanism of Bi₂Te₃, we examine the deformation process of single crystalline Bi₂Te₃. We used DFT to determine the shear-stress – shear-strain relationships of single crystalline Bi₂Te₃ along various directions within the (001) cleavage plane, as shown in Figure 2(a). Each slip system shows an extremely low ideal shear strength of

- 0.16 GPa for the (001)/<502> slip system,
- 0.19 GPa for the (001)/<50-1> slip system, and
- 0.22 GPa for the (001)/<210> slip system.

This agrees well with the experimental observation that Bi₂Te₃ easily cleaves along the (00 l) plane [35,36]. Beyond the maximum shear stress point, each slip system exhibits an obvious ‘yielding’ stage, indicating a softening structural stiffness. To determine bond-response processes, we extracted the atomic configurations at critical strains and bond length changes, as shown in Figure 2(b)-(d). The **van der Waals** Te1–Te1 interactions dominate the ideal shear strength and its deformation modes of crystalline Bi₂Te₃. Along the (001)/<50-1> slip system, the weak **van der Waals** Te1–Te1 interatomic distance stretches rapidly, with a bond stretching ratio of 42.5% at 0.22 shear strain. The Bi–Te1 and Bi–Te2 bonds exhibit negligible stretching, suggesting that the

Te1–Bi–Te2–Bi–Te1 substructure remains intact during the shear process. The atomic structures show clearly that the Te1–Te1 bond resists external deformation while the Te1–Bi–Te2–Bi–Te1 substructure holds together. These deformation modes for the (001)/<502> and (001)/<210> slip systems are similar as shown in Figures S3 and S4 in the Supporting Information (SI) [39].

We find that nanotwins in Bi_2Te_3 dramatically change the material's strength and its deformation mechanisms. To illustrate these effects, we used DFT to probe the shear deformation of the nanotwinned Bi_2Te_3 along the TBs, as shown in Figure 3. In the elastic stage with shear strain less than 4%, the slope of the stress-strain response for nanotwinned Bi_2Te_3 is 59% higher than that of single crystalline Bi_2Te_3 , illustrating the strengthening effect of the nanotwins. Indeed, we find that nanotwinned Bi_2Te_3 displays an ideal shear stress of 0.60 GPa, which is more than three times higher than that of single crystalline Bi_2Te_3 (0.19 GPa). This suggests that nanotwins can superstrengthen Bi_2Te_3 . In addition, the sudden drop of shear stress in twinned Bi_2Te_3 (Figure 3(a)) indicates the brittle failure, totally different from the plastic deformation in single crystalline Bi_2Te_3 . These can be attributed to intriguing bond rearrangements near the TBs. The newly formed Te1(1)–Te1(2) and Te1(2)–Te1(3) bonds (3.48 Å), which are considered weak covalent bonds, strengthen the interactions between different substructures. When nanotwinned Bi_2Te_3 is sheared (Figure 3(c)), the lower half part shears along the same shear direction as single crystalline Bi_2Te_3 , leading to the stretching of the Te1(2)–Te1(3) and Te1(6)–Te1(7) bonds (Figure 3(b)). However, the upper half part shears along the opposite shear direction, leading to a compression of the Te1(1)–Te1(2) and Te1(4)–Te1(5) bonds (Figure 3(b)). The newly formed Te1(2)–Te1(3) bond has a much smaller stretching ratio than the **van der Waals** Te1(6)–Te1(7) bond, indicating the Te1(2)–Te1(3) bond is much stronger than the Te1(6)–Te1(7) bond in resisting external deformation, resulting in the strengthening effect of nanotwins at the elastic stage as shown in Figure 3(a). Moreover, the strong Te1(1)–Te1(2) and Te1(2)–Te1(3) bonds suppress the softening of the **van der Waals** Te1–Te1 bonds near the TBs, giving rise to the super-strengthened nanotwin (0.60 GPa) compared to the single crystal (0.19 GPa). **The shear strain (0.123) corresponding to the mechanical strength in nanotwinned Bi_2Te_3 is much larger than that (0.071) in single crystalline Bi_2Te_3 . This strain-stiffening effect would lead to the potential better manufacturability of this nanotwin.** This effect is similarly found in inorganic crystalline solids [41], where the enhanced material's strength mainly arises from newly formed atomic bonds under large structural deformations. At 0.134 shear strain, the Te1(2)–Te1(3) bond stretching ratio sharply increases from 8% to 17%. This indicates a highly softening or non-bonding interaction (Figure 3(d)), leading to a sudden drop of the shear stress (Figure 3(a)). As

shear strain increases to 0.145, the Te1(1)–Te1(2) bond breaks, destabilizing the TBs and resulting in structural failure (Figure 3(e)). **This clearly suggests that this robust nanotwin leads to less plasticity compared with single crystalline Bi₂Te₃.**

In the other two nanotwinned Bi₂Te₃ structures (Figure S5-S6 in SI) [39], the nanotwins have no obvious influence on the mechanical properties because the TBs do not change the interaction between the Te1–Bi–Te2–Bi–Te1 substructures which are coupled through their **van der Waals** Te1–Te1 interactions.

Here, we compared the ideal shear strength of Bi₂Te₃ with various high-performance TE materials [34,42–45]. As shown in Figure 4, Bi₂Te₃ has the lowest ideal shear strength (0.19 GPa) among all these TE materials, which can be attributed to the layered structure with very weak **van der Waals** Te1–Te1 interactions. The calculated stretching force constant (SFC) [46] of Te1–Te1 bond using ATAT code [47] is only 0.25 eV/Å², which is much lower than those of the Bi–Te2 bond (0.62 eV/Å²) and Bi–Te1 bond (2.24 eV/Å²). This well explains that the Te1–Te1 bond is highly stretched to resist the deformation while the Te1–Bi–Te2–Bi–Te1 five-layer substructure holds together (Figure 2), which is similarly found in layered SnSe [42]. Thus, Bi₂Te₃ and SnSe exhibit low ideal strengths of 0.19 and 0.59 GPa, respectively, because the **van der Waals**-like bonding interactions dominate the shear deformations. In La₃Te₄, Mg₃Sb₂, CaMg₂Sb₂, and CaZn₂Sb₂, the ionic bonds are responsible for the ideal strength and deformation modes [43,44], leading to a higher ideal strength compared with that in Bi₂Te₃, as shown in Figure 4. Moreover, due to the strong covalent Co–Sb 3D framework in CoSb₃ and even much stronger TiSn 3D framework in TiNiSn, CoSb₃ and TiNiSn show an extremely high ideal strength of 7.17 and 10.52 GPa, respectively [34,45].

The weak **van der Waals** interaction between Te1–Bi–Te2–Bi–Te1 substructures leads to a significantly low ideal strength in bulk Bi₂Te₃. However, in nanotwinned Bi₂Te₃, a newly formed covalent bond in the vicinity of TBs can remarkably enhance the coupling interaction between different substructures, which strongly improves the structural stiffness. This suppresses the structural softening and strengthens the material as embedded in Figure 4. This structure-stiffening mechanism can well explain recent experimental results reporting that Bi₂Te₃ with TBs shows an eight-fold and a six-fold increase in the compressive and flexural strength, respectively, compared with those of single crystalline Bi₂Te₃ [29]. **This strengthening effect in Bi₂Te₃ TE semiconductor, which arises from the bonding in the TB, is similar with De Jong *et al.*'s finding that the local structure and bonding in the TB vicinity are useful in controlling the mechanical behavior of transition metals [48].** Our results show that the rapidly stretched **van der Waals** bond

leads to the softening and the failure of Bi_2Te_3 . Thus, it is unlikely that this robust nanotwin can be formed through deformation. We expect that they can be introduced during the growth or melt processes, such as melt spinning combined with a plasma-activated sintering [29].

The mechanical properties of real samples of Bi_2Te_3 are closely related to defects such as GBs and vacancies that are ubiquitous in real materials. Studying GB effects requires cell sizes much larger than practical for DFT. Thus, future studies fitting the DFT results in this Letter to a Reactive force field for molecular dynamics simulations will be useful for testing how such defects affect the strength.

Here we examined how nanotwins influence the mechanical properties of Bi_2Te_3 TE material. Previous experimental studies showed that nanotwins could be used to tailor the electronic structure and to suppress the lattice thermal conductivity of Bi_2Te_3 [29,40]. This is worthy of future studies.

In summary, we applied DFT to determine the role of nanotwins on mechanical properties of Bi_2Te_3 revealing that the newly generated Te1–Te1 covalent bonds in the vicinity of the twin boundary significantly improves the coupling interaction between Te1–Bi–Te2–Bi–Te1 five-layer substructures. Formation of nanotwins remarkably enhances the structural stiffness while suppressing the structure softening, leading to a much higher ideal strength of 0.6 GPa in nanotwinned Bi_2Te_3 compared to that of the single crystalline Bi_2Te_3 (0.19 GPa). Our work proposes a new TB engineering strategy to enhance the mechanical integrity of Bi_2Te_3 , where the stronger structural stiffness can be achieved by a structural modification rather than a traditional elemental doping. This work opens a new pathway to rationally design robust high-performance TE materials, which can be also applied to other TE or non-TE energy materials.

Other exciting application of Bi_2Te_3 is as topological insulators (TI) [49]. Goddard *et al.* have shown theoretically that Bi_2Te_3 is TI, with spectacular states in the gap for Bi_2Te_3 [50]. It may be that the incorporation of the TBs could modulate the TI properties while strengthening the materials.

This work is partially supported by National Basic Research Program of China (973-program) under Project no. 2013CB632505, the 111 Project of China under Project no. B07040, Materials Project by Department of Energy Basic Energy Sciences Program under Grant No. EDCBEE, DOE Contract DE-AC02-05CH11231, and China Postdoctoral Science Foundation (408-32200031). We would like to acknowledge the Jet Propulsion Laboratory, California Institute of Technology, as a funding source under a contract with the National Aeronautics and Space Administration, which was supported by the NASA Science Missions Directorate's Radioisotope Power Systems Technology Advancement Program. Q.A. was supported by U. S.

Nuclear Regulatory Commission (NRC) under Cooperative Agreement Number NRC-HQ-84-15-G-0028. S.M. was supported by Act 211 Government of the Russian Federation, Contract No. 02.A03.21.0011 and by the Supercomputer Simulation Laboratory of South Ural State University [51]. Support for W.A.G. and the computing was provided by supported NSF (DMR-1436985).

REFERENCES

- [1] G. J. Snyder and E. S. Toberer, *Nat. Mater.* **7** (2), 105 (2008).
- [2] Y. Z. Pei, X. Y. Shi, A. LaLonde, H. Wang, L. D. Chen, and G. J. Snyder, *Nature*. **473** (7345), 66 (2011).
- [3] Y. L. Tang, Z. M. Gibbs, L. A. Agapito, G. Li, H. S. Kim, M. B. Nardelli, S. Curtarolo, and G. J. Snyder, *Nat. Mater.* **14** (12), 1223 (2015).
- [4] J. W. Zhang, L. R. Song, S. H. Pedersen, H. Yin, L. T. Hung, and B. B. Iversen, *Nat. Commun.* **8**, 13901 (2017).
- [5] M. S. El-Genk, H. H. Saber, T. Caillat, and J. Sakamoto, *Energ. Convers. Manage.* **47** (2), 174 (2006).
- [6] D. G. Zhao, H. R. Geng, and L. D. Chen, *Int. J. Appl. Ceram. Tec.* **9** (4), 733 (2012).
- [7] K. H. Bae, S. M. Choi, K. H. Kim, H. S. Choi, W. S. Seo, I. H. Kim, S. Lee, and H. J. Hwang, *J. Electron. Mater.* **44** (6), 2124 (2015).
- [8] X. L. Su, P. Wei, H. Li, W. Liu, Y. G. Yan, P. Li, C. Q. Su, C. J. Xie, W. Y. Zhao, P. C. Zhai, Q. J. Zhang, X. F. Tang, and C. Uher, *Adv. Mater.* **29** (20), 1602013 (2017).
- [9] H. J. Goldsmid, *Materials*. **7** (4), 2577 (2014).
- [10] L. P. Hu, T. J. Zhu, X. H. Liu, and X. B. Zhao, *Adv. Func. Mater.* **24** (33), 5211 (2014).
- [11] X. Shi, J. Yang, J. R. Salvador, M. F. Chi, J. Y. Cho, H. Wang, S. Q. Bai, J. H. Yang, W. Q. Zhang, and L. D. Chen, *J. Am. Chem. Soc.* **133** (20), 7837 (2011).
- [12] G. Rogl and P. Rogl, *Sci. Adv. Mater.* **3** (4), 517 (2011).
- [13] L. D. Zhao, B. P. Zhang, J. F. Li, M. Zhou, W. S. Liu, and J. Liu, *J. Alloy. Compd.* **455** (1-2), 259 (2008).
- [14] E. O. Hall, *P. Phys. Soc. Lond. B.* **64** (381), 747 (1951).
- [15] N. J. Petch, *J. Iron. Steel. I.* **174** (1), 25 (1953).
- [16] J. Schiøtz and K. W. Jacobsen, *Science*. **301** (5638), 1357 (2003).
- [17] T. J. Rupert, D. S. Gianola, Y. Gan, and K. J. Hemker, *Science*. **326** (5960), 1686 (2009).
- [18] K. Lu, L. Lu, and S. Suresh, *Science*. **324** (5925), 349 (2009).
- [19] K. M. Reddy, J. J. Guo, Y. Shinoda, T. Fujita, A. Hirata, J. P. Singh, J. W. McCauley, and M. W. Chen, *Nat. Commun.* **3**, 1052 (2012).
- [20] Q. An, K. M. Reddy, J. Qian, K. J. Hemker, M. W. Chen, and W. A. Goddard, *Nat. Commun.* **7**, 11001 (2016).

- [21] Q. An, W. A. Goddard, K. Y. Xie, G. D. Sim, K. J. Hemker, T. Munhollon, M. F. Toksoy, and R. A. Haber, *Nano. Lett.* **16** (12), 7573 (2016).
- [22] L. Lu, X. Chen, X. Huang, and K. Lu, *Science*. **323** (5914), 607 (2009).
- [23] Q. Huang, D. L. Yu, B. Xu, W. T. Hu, Y. M. Ma, Y. B. Wang, Z. S. Zhao, B. Wen, J. L. He, Z. Y. Liu, and Y. J. Tian, *Nature*. **510** (7504), 250 (2014).
- [24] Y. J. Tian, B. Xu, D. L. Yu, Y. M. Ma, Y. B. Wang, Y. B. Jiang, W. T. Hu, C. C. Tang, Y. F. Gao, K. Luo, Z. S. Zhao, L. M. Wang, B. Wen, J. L. He, and Z. Y. Liu, *Nature*. **493** (7432), 385 (2013).
- [25] S. Il Kim, K. H. Lee, H. A. Mun, H. S. Kim, S. W. Hwang, J. W. Roh, D. J. Yang, W. H. Shin, X. S. Li, Y. H. Lee, G. J. Snyder, and S. W. Kim, *Science*. **348** (6230), 109 (2015).
- [26] X. Meng, Z. Liu, B. Cui, D. Qin, H. Geng, W. Cai, L. Fu, J. He, Z. Ren, and J. Sui, *Adv. Energ. Mater.* 1602582 (2017).
- [27] J. Z. Xin, H. J. Wu, X. H. Liu, T. J. Zhu, G. T. Yu, and X. B. Zhao, *Nano. Energy*. **34**, 428 (2017).
- [28] Z. W. Chen, B. H. Ge, W. Li, S. Q. Lin, J. W. Shen, Y. J. Chang, R. Hanus, G. J. Snyder, and Y. Z. Pei, *Nat. Commun.* **8**, 13828 (2017).
- [29] Y. Zheng, Q. Zhang, X. L. Su, H. Y. Xie, S. C. Shu, T. L. Chen, G. J. Tan, Y. G. Yan, X. F. Tang, C. Uher, and G. J. Snyder, *Adv. Energy. Mater* **5** (5), 1401391 (2015).
- [30] G. Kresse and J. Furthmuller, *Comp. Mater. Sci.* **6** (1), 15 (1996).
- [31] G. Kresse and J. Furthmuller, *Phys. Rev. B.* **54** (16), 11169 (1996).
- [32] G. Kresse and D. Joubert, *Phys. Rev. B.* **59** (3), 1758 (1999).
- [33] J. P. Perdew, K. Burke, and M. Ernzerhof, *Phys. Rev. Lett.* **77** (18), 3865 (1996).
- [34] G. D. Li, Q. An, W. J. Li, W. A. Goddard, P. C. Zhai, Q. J. Zhang, and G. J. Snyder, *Chem. Mater.* **27** (18), 6329 (2015).
- [35] M. H. Francombe, *Brit. J. Appl. Phys.* **9** (10), 415 (1958).
- [36] J. R. Wiese and L. Muldower, *J. Phys. Chem. Solids.* **15** (1-2), 13 (1960).
- [37] M. de Jong, W. Chen, T. Angsten, A. Jain, R. Notestine, A. Gamst, M. Sluiter, C. K. Ande, S. van der Zwaag, J. J. Plata, C. Toher, S. Curtarolo, G. Ceder, K. A. Persson, and M. Asta, *Sci. Data.* **2**, 150009 (2015).
- [38] V. V. Atuchin, T. A. Gavrilova, K. A. Kokh, N. V. Kuratieva, N. V. Pervukhina, and N. V. Surovtsev, *Solid. State. Commun.* **152** (13), 1119 (2012).
- [39] See Supplemental Material for a detailed description of Nanotwinned Bi_2Te_3 structure with the TB along the $\{70\bar{1}\}$ and $\{210\}$ plane, respectively; Bond-responding process of single crystalline Bi_2Te_3 along the $(001)/\langle 502 \rangle$ and $(001)/\langle 210 \rangle$ slip system, respectively; Deformation modes of nanotwinned Bi_2Te_3 with TB along the $\{70\bar{1}\}$ and $\{210\}$ plane, respectively.
- [40] K. C. Kim, J. Lee, B. K. Kim, W. Y. Choi, H. J. Chang, S. O. Won, B. Kwon, S. K. Kim, D. B. Hyun, H. J. Kim, H. C. Koo, J. H. Choi, D. I. Kim, J. S. Kim, and S. H. Baek, *Nat. Commun.* **7**, 12449 (2016).
- [41] C. Jiang and S. G. Srinivasan, *Nature*. **496** (7445), 339 (2013).

- [42] G. Li, U. Aydemir, M. Wood, W. A. Goddard, P. C. Zhai, Q. J. Zhang, and G. J. Snyder, *Chem. Mater.* **29** (5), 2382 (2017).
- [43] G. Li, U. Aydemir, M. Wood, W. A. Goddard, P. Zhai, Q. Zhang, and G. J. Snyder, *J. Phys. D: Appl. Phys.* **50** (27), 274002 (2017).
- [44] G. Li, U. Aydemir, M. Wood, Q. An, W. A. Goddard, P. Zhai, Q. Zhang, and G. J. Snyder, *J. Mater. Chem. A.* **5** (19), 9050 (2017).
- [45] G. D. Li, Q. An, U. Aydemir, W. A. Goddard, M. Wood, P. C. Zhai, Q. J. Zhang, and G. J. Snyder, *J. Mater. Chem. A.* **4** (38), 14625 (2016).
- [46] The calculation of a stretching force constant is similar to frozen phonon calculations. The stretching force constant is calculated by fitting a spring model to the force matrix resulting from imposed atomic displacements. In each perturbed system, only a small atomic displacement (0.1 Å in our calculation) was imposed along each direction ($\pm x$, $\pm y$, or $\pm z$). The total energy is evaluated for each system with a displacement pattern, and the force constant matrix is obtained by the derivatives of the total energy with respect to the displacement.
- [47] A. van de Walle, M. Asta, and G. Ceder, *Calphad.* **26** (4), 539 (2002).
- [48] M. de Jong, J. Kacher, M. H. Sluiter, L. Qi, D. L. Olmsted, A. van de Walle, J. W. Morris, A. M. Minor, and M. Asta, *Phys. Rev. Lett.* **115** (6), 065501 (2015).
- [49] Y. L. Chen, J. G. Analytis, J. H. Chu, Z. K. Liu, S. K. Mo, X. L. Qi, H. J. Zhang, D. H. Lu, X. Dai, Z. Fang, S. C. Zhang, I. R. Fisher, Z. Hussain, and Z. X. Shen, *Science.* **325** (5937), 178 (2009).
- [50] J. M. Crowley, J. Tahir-Kheli, and W. A. Goddard, *J. Phys. Chem. Lett.* **6** (19), 3792 (2015).
- [51] P.S. Kostenetskiy, A.Y. Safonov, SUSU Supercomputer Resources. Proceedings of the 10th Annual International Scientific Conference on Parallel Computing Technologies (Arkhangelsk, Russia, 2016).

Figure 1.

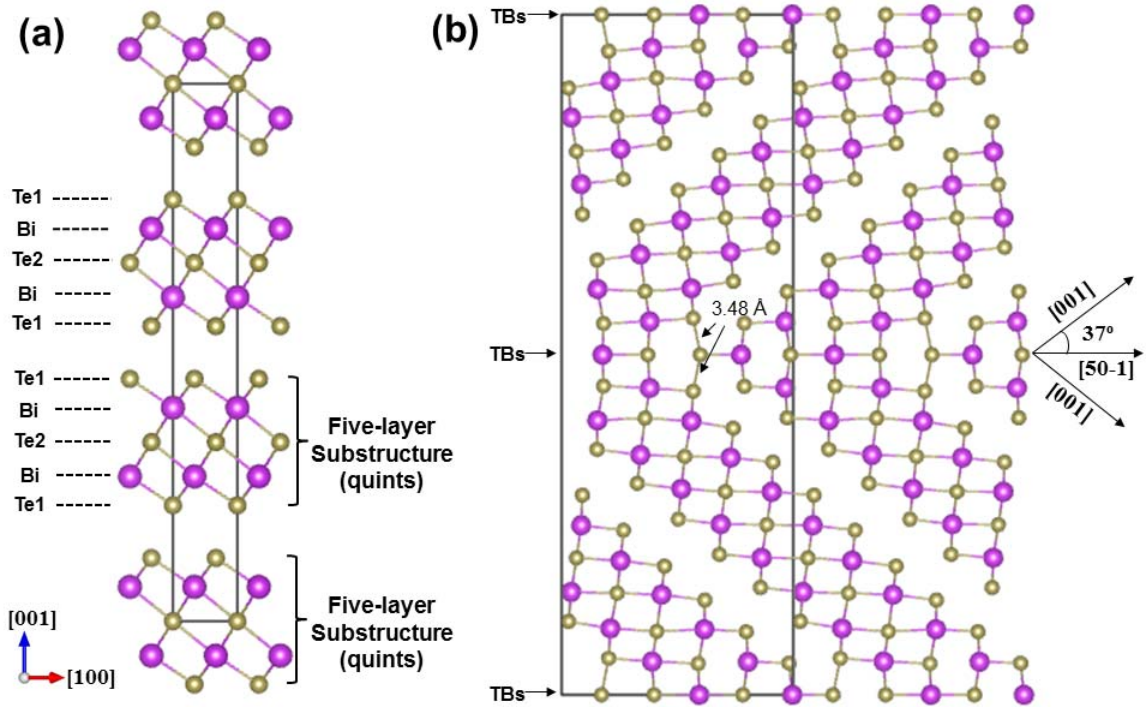


Figure 1. (a) Crystal structure of untwinned Bi_2Te_3 showing the hexagonal unit cell, which consists of Te1–Bi–Te2–Bi–Te1 quint (five-layer substructure) along the $[001]$ axis. The hexagonal unit cell contains $6 \times \text{Bi}$ and $9 \times \text{Te}$ atoms, which are shown in purple and light yellow spheres, respectively. (b) Nanotwinned Bi_2Te_3 structure with the TB along the $\{702\}$ plane. The unit cell contains $40 \times \text{Bi}$ and $60 \times \text{Te}$ atoms. The measured angle on each side of the TBs is 37° , and the twinning size is 2.4 nm. The black rectangle region represents the unit cell in nanotwinned Bi_2Te_3 . The weak covalent Te1–Te1 bond ($d_{\text{Te1-Te1}} = 3.48 \text{ \AA}$) in Figure 1(b) is much stronger than the **van der Waals** Te1–Te1 interactions ($d_{\text{Te1-Te1}} = 3.82 \text{ \AA}$) in Figure 1(a).

Figure 2.

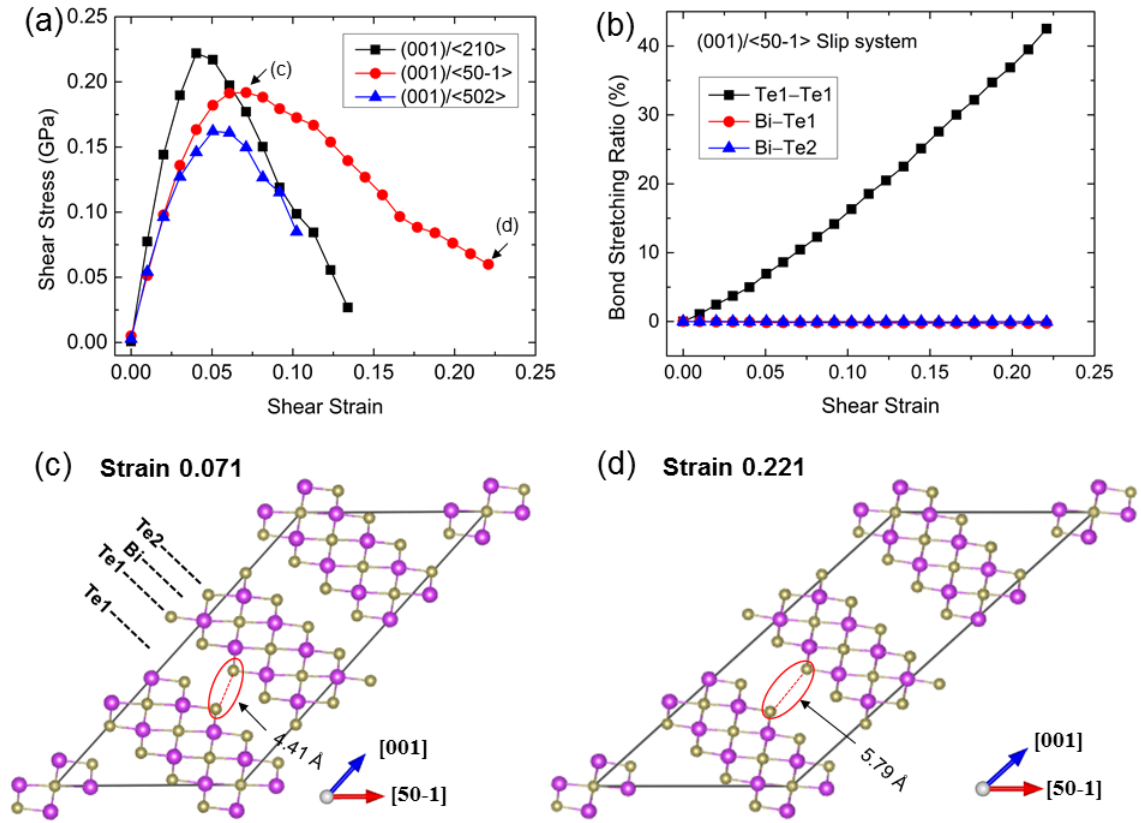


Figure 2. Deformation behavior of single crystalline Bi_2Te_3 . (a) The shear-stress–shear-strain relationships under shear deformation along various slip systems. (b) The bond stretching ratio (Te1–Te1, Bi–Te1, Bi–Te2) with increasing shear strain along the $(001)/\langle 50-1 \rangle$ slip system. (c) The atomic structure at 0.071 shear strain corresponding to the maximum shear stress along the $(001)/\langle 50-1 \rangle$ slip system. (d) The atomic structure at 0.221 shear strain corresponding to highly softening Te1–Te1 bond along the $(001)/\langle 50-1 \rangle$ slip system. The red dashed lines and red ellipses displayed in Figure 2(c)-(d) highlight the **van der Waals** Te1–Te1 bond softening.

Figure 3.

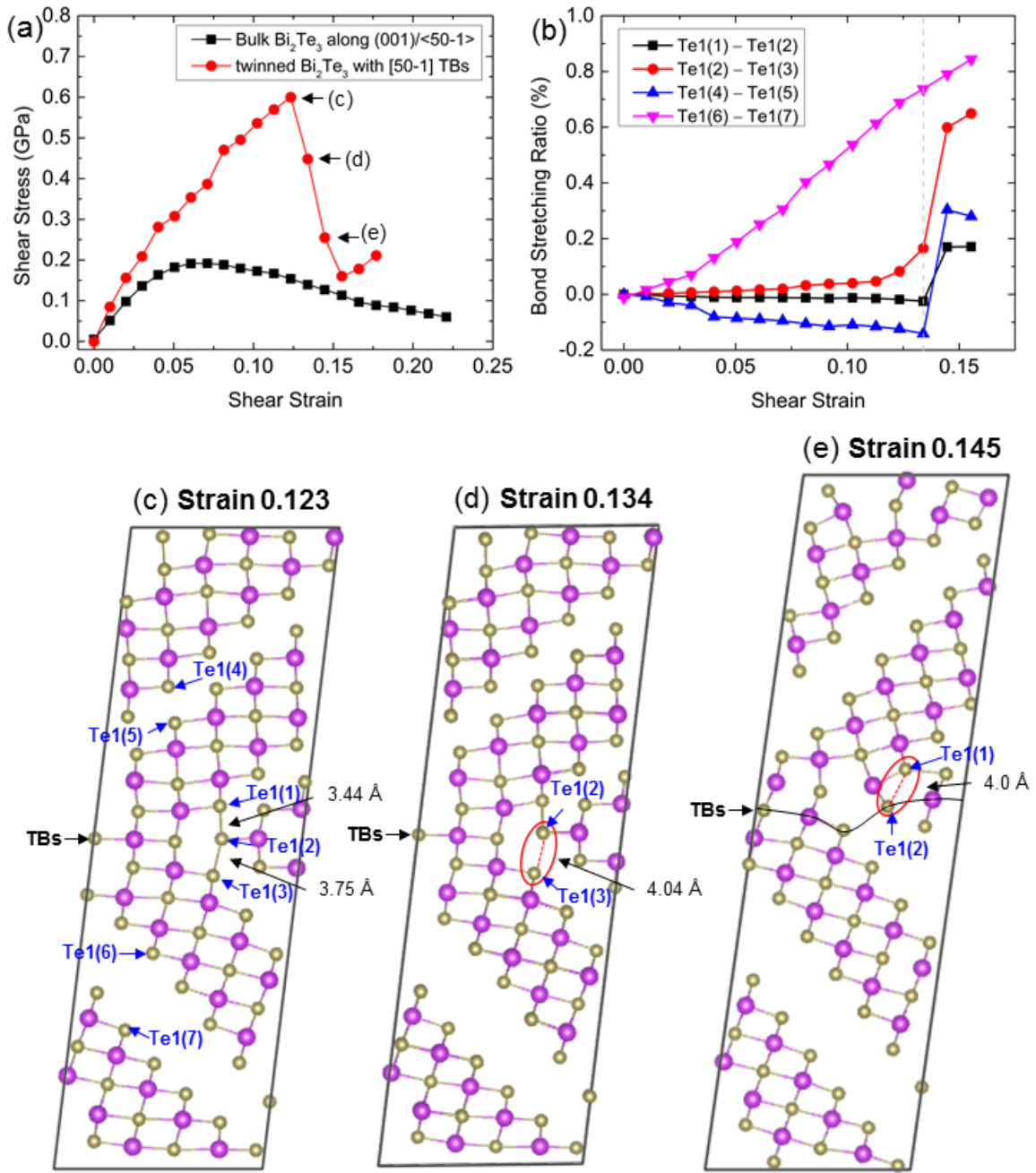


Figure 3. Deformation modes of nanotwinned Bi_2Te_3 with TBs along the $\{702\}$ plane. (a) The shear-stress – shear-strain relationships of nanotwinned Bi_2Te_3 compared with single crystalline Bi_2Te_3 . (b) The bond stretching ratio (Te1(1)–Te1(2), Te1(2)–Te1(3), Te1(4)–Te1(5), Te1(6)–Te1(7)) with the increasing shear strain. (c) The atomic structure at 0.123 shear strain corresponding to the maximum shear stress. (d) The

atomic structure at 0.134 shear strain corresponding to the breakage of Te1(2)–Te1(3) bond. (e) The atomic structure at 0.145 shear strain corresponding to the structural failure. The gray dashed line in Figure 3(b) represents the critical strain before failure. The red ellipses displayed in Figure 3(d)-(e) highlight the breakage of Te1(2)–Te1(3) and Te1(1)–Te1(2) bonds. The black curve in Figure 3(e) guides the collapsed TBs.

Figure 4.

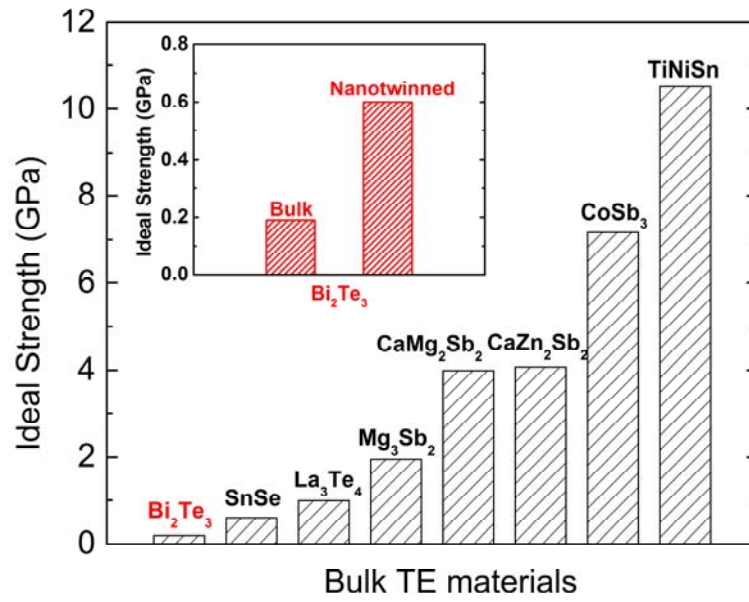


Figure 4. The ideal shear strength for various high-performance bulk TE materials: (single crystalline) Bi_2Te_3 , SnSe [42], La_3Te_4 [43], Mg_3Sb_2 [44], CaMg_2Sb_2 [44], CaZn_2Sb_2 [44], CoSb_3 [34], and TiNiSn [45]. The embedded figure shows the ideal strength of bulk and nanotwinned Bi_2Te_3 .